ELSEVIER

Powder Technology 125 (2002) 45–54

POWDER TECHNOLOGY

www.elsevier.com/locate/powtec

An experimental and numerical study of the angle of repose of coarse spheres

Y.C. Zhou [a], B.H. Xu [a], A.B. Yu [a,*], P. Zulli [b]

[a] *Centre for Computer Simulation and Modelling of Particulate Systems, School of Materials Science and Engineering, The University of New South Wales, Sydney, NSW 2052, Australia*

[b] *BHP Steel Research Laboratories, P.O. Box 202, Port Kembla, NSW 2505, Australia*

Received 30 July 2001; received in revised form 1 October 2001; accepted 29 November 2001

Abstract

This paper presents a numerical and experimental study of the angle of repose of mono-sized coarse spheres, a most important macroscopic parameter in characterising granular materials. Numerical experiments are conducted by means of a modified discrete element method. Emphasis is given to the effects of variables related to factors such as particle characteristics, material properties and geometrical constraints. The results show that under the present simulation conditions, the angle of repose is significantly affected by the sliding and rolling frictions, particle size and container thickness, and is not sensitive to density, Poisson's ratio, damping coefficient and Young's modulus. Increasing rolling or sliding friction coefficient increases the angle of repose, while increasing particle size or container thickness decreases the angle of repose. Based on the numerical results, empirical equations are formulated for engineering application. The proposed simulation technique and equations are validated by comparing the physical and numerical experiments, where focus is given to the effects of particle size and container thickness.

Keywords: Angle of repose; Sandpile; Granular material; Discrete element method

1. Introduction

The angle of repose is one of the most important macroscopic parameters in characterising the behaviour of granular materials. It is related to many important phenomena, including avalanching [1–3], stratification [4,5] and segregation [6–8], and is therefore a research focus for years. It has been found that the angle of repose strongly depends on material properties such as sliding and rolling frictions [9–11] and density of particles [12], and particle characteristics such as size [8,13] and shape [12,14], in addition to the method of formating a sandpile to form a sandpile [15,16]. It is generally reported that the angle of repose increases with increasing sliding and rolling friction coefficients and deviation from spheres, and decreases with increasing particle size and container thickness. However, quantitative description of the dependence that can be used generally in engineering practice is not available.

The bulk behaviour of a particle system depends on the collective interactions of individual particles, and hence particle scale analysis plays a critical role in elucidating the underlying mechanisms of the effects mentioned above. In the past, various modelling techniques have been used to investigate the behaviour of particles in granular media at such a scale, including Monte Carlo (MC) [17,18], Cellular Automaton (CA) [19,20], and Discrete Element Method (DEM) [21,22]. Amongst these techniques, DEM is probably the most realistic one, because it explicitly takes into account not only the geometrical factors but also the forces involved in the formation of a sandpile. Previous DEM studies are largely limited to two-dimensional and also suffer the problem of stabilising a heap composed of spheres as there is no mechanism to stop spheres from rolling [9,23]. We have recently found that this problem can be solved with the incorporation of a rolling friction model into the DEM [11]. The resulting modified DEM would provide an effective way to study the angle of repose and the complex dynamic internal state of sandpiles under well controlled conditions.

This paper reports such a numerical and experimental study of the angle of repose of coarse particles. The effects of key variables such as rolling friction coefficient, sliding

* Corresponding author. Fax: +61-2-9385-5956.
E-mail address: a.yu@unsw.edu.au (A.B. Yu).

0032-5910/02/$ - see front matter
PII: S0032-5910(01)00520-4

friction coefficient, particle size and container thickness is first presented. A predictive equation is then formulated based on the numerical results and validated by physical experiments conducted under comparable conditions.

2. DEM simulation

The simulations were performed based on the DEM originally proposed by Cundall and Strack [21] but modified by incorporating a rolling friction model in the rotational equation of a particle [11]. According to this model, the translational and rotational motions of particle i in a system at time t, caused by its interactions with neighbouring particles or walls, can be described by the following equations:

$$m_i \frac{dV_i}{dt} = m_i \boldsymbol{g} + \sum_{j=1}^{k_i} (\boldsymbol{F}_{\mathrm{cn},ij} + \boldsymbol{F}_{\mathrm{dn},ij} + \boldsymbol{F}_{\mathrm{ct},ij} + \boldsymbol{F}_{\mathrm{dt},ij}) \qquad (1)$$

and

$$I_i \frac{d\omega_i}{dt} = \sum_{j=1}^{k_i} (\boldsymbol{T}_{ij} + \boldsymbol{M}_{ij}) \qquad (2)$$

where m_i, I_i, $\boldsymbol{V}_i$ and ω_i are, respectively, the mass, moment of inertia, translational and rotational velocities of particle i. The forces involved are the gravitational force, $m_i\boldsymbol{g}$, and inter-particle forces between particles i and j, which include the contact forces $\boldsymbol{F}_{\mathrm{cn},ij}$ and $\boldsymbol{F}_{\mathrm{dn},ij}$, and viscous contact damping forces $\boldsymbol{F}_{\mathrm{ct},ij}$ and $\boldsymbol{F}_{\mathrm{dt},ij}$. The inter-particle forces are summed over the k_i particles in contact with particle i and dependent on the normal and tangential deformation, δ_{n} and δ_{t}. Torques, $\boldsymbol{T}_{ij}$, are generated by tangential forces and cause particle i to rotate, because the inter-particle forces act at the contact point between particles i and j and not at the particle centre. $\boldsymbol{M}_{ij}$ are the rolling friction torques that oppose to the rotation of the ith particle, which arises from the resulting elastic hysteresis loss and time-dependent deformation [24]. The formulations used to calculate the forces and torques in Eqs. (1) and (2) are listed in Table 1. Eqs. (1) and (2) can be solved numerically by a finite difference method.

Simulations were carried out in a rectangular container with a fixed middle plate and two side outlets by using the discharging method in connection with our previous study [11]. Its geometrical details are shown in Fig. 1. The container size can be scaled up or down corresponding to the particle diameter used. Furthermore, to study the wall effect observed by Grasselli and Herrmann [15] and Dury et al. [8], the container thickness was also adjustable; in some simulations, periodic boundary conditions were applied to the front and rear walls.

A simulation was started with the random generation of spheres without overlaps in the container above the fixed middle plate with two outlets closed, followed by a gravitational settling process for 1.0 s to form a stable packing (Fig. 1a). Then, the instantaneous opening of the outlets started a discharging process in which spheres dropped into the bottom of the container under gravity. Some spheres remained on the middle plate after the discharging, forming a stable sandpile (Fig. 1b). The angle of repose could then be determined from the surface profile of the pile with a measurement error within 2 degrees. Table 2 lists the variables considered in this study. For convenience, unless otherwise specified, the effect of a variable was considered within a certain range while other variables were fixed, giving a so-called base condition (Table 2).

3. Experimental work

To examine the validity of the proposed simulation technique, physical experiments were carried out under

Table 1
Components of forces and torque acting on particle i

Forces and torques		Symbols	Equations
Normal forces	Contact	$\boldsymbol{F}_{\mathrm{cn},ij}$	$-\frac{4}{3}E^*\sqrt{\mathrm{R}^*}\,\delta_{\mathrm{n}}^{\frac{3}{2}}\mathbf{n}$
	Damping	$\boldsymbol{F}_{\mathrm{dn},ij}$	$-c_{\mathrm{n}}\left(6m_{ij}E^*\sqrt{\mathrm{R}^*\delta_{\mathrm{n}}}\right)^{\frac{1}{2}}\boldsymbol{V}_{n,ij}$
Tangential forces	Contact	$\boldsymbol{F}_{\mathrm{ct},ij}$	$-\frac{\mu_{\mathrm{s}}\lvert\boldsymbol{F}_{\mathrm{cn},ij}\rvert}{\lvert\boldsymbol{\delta}_{\mathrm{t}}\rvert}\left[1-\left(1-\frac{\min\{\lvert\boldsymbol{\delta}_{\mathrm{t}}\rvert,\,\delta_{\mathrm{t,max}}\}}{\delta_{\mathrm{t,max}}}\right)^{\frac{3}{2}}\right]\boldsymbol{\delta}_{\mathrm{t}}$
	Damping	$\boldsymbol{F}_{\mathrm{dt},ij}$	$-c_{\mathrm{t}}\left(6m_{ij}\mu_{\mathrm{s}}\lvert\boldsymbol{F}_{\mathrm{cn},ij}\rvert\frac{\sqrt{1-\lvert\boldsymbol{\delta}_{\mathrm{t}}\rvert/\delta_{\mathrm{t,max}}}}{\delta_{\mathrm{t,max}}}\right)^{\frac{1}{2}}\boldsymbol{V}_{\mathrm{t},ij}$
Rolling	Torque	$\boldsymbol{T}_{ij}$	$\boldsymbol{R}_i\times(\boldsymbol{F}_{\mathrm{ct},ij}+\boldsymbol{F}_{\mathrm{dt},ij})$
	Friction torque	$\boldsymbol{M}_{ij}$	$-\mu_{\mathrm{r}}\lvert\boldsymbol{F}_{\mathrm{cn},ij}\rvert\hat{\boldsymbol{\omega}}_i$
Gravity		$\boldsymbol{G}_i$	$m_i\boldsymbol{g}$

Where: $\frac{1}{\mathrm{R}^*}=\frac{1}{|\boldsymbol{R}_i|}+\frac{1}{|\boldsymbol{R}_j|}$, $E^*=\frac{E}{2(1-\nu^2)}$, $\hat{\boldsymbol{\omega}}_i=\frac{\boldsymbol{\omega}_i}{|\boldsymbol{\omega}_i|}$, $\mathbf{n}=\frac{\boldsymbol{R}_i}{|\boldsymbol{R}_i|}$, $\delta_{\mathrm{t,max}}=\mu_{\mathrm{s}}\frac{2-\nu}{2(1-\nu)}\delta_{\mathrm{n}}$ $\boldsymbol{V}_{ij}=\boldsymbol{V}_j-\boldsymbol{V}_i+\boldsymbol{\omega}_j\times\boldsymbol{R}_j-\boldsymbol{\omega}_i\times\boldsymbol{R}_i$, $\boldsymbol{V}_{\mathrm{n},ij}=(\boldsymbol{V}_{ij}\cdot\mathbf{n})\cdot\mathbf{n}$, $\boldsymbol{V}_{\mathrm{t},ij}=(\boldsymbol{V}_{ij}\times\mathbf{n})\times\mathbf{n}$.

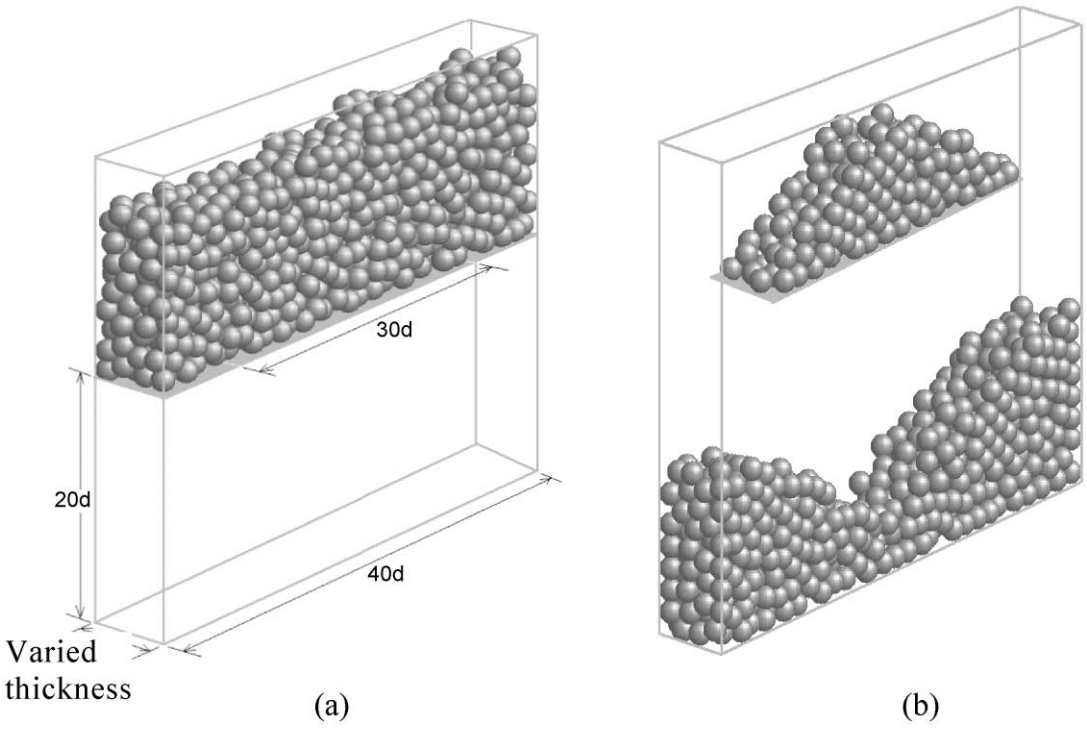

Fig. 1. Geometry and formation of a sandpile; d is particle diameter: (a), before discharging; (b), after discharging.

conditions comparable to those used in the simulation. The container was made of wooden except for the front wall that was made of perspex for visual observation. Glass beads with diameters of 0.55, 1, 2, 5 and 10 mm (particle density = 2500 kg/m^3) were employed in the experiments. They are reasonably monosized, except for the 0.55 beads whose size ranges from 0.495 to 0.6 mm. Because of this, the comparison between numerical and experimental results were just made for coarser beads.

The container used in the experimental work has a fixed size except for its thickness. The width and height are both 400 mm. The container thickness can be scaled up or down with particle size. An experiment was started by filling the glass beads into the container above the middle plate with the depth of the glass beads at 150 mm. Then the two outlets were opened simultaneously and a stable sandpile was formed on the middle plate. For the same-sized particles, at least six sandpiles were constructed with the container thickness ranged approximately from 4d to 36d. Each sandpiling process was repeated three times to generate an averaged angle of repose. A video camera was used to record the whole discharge process.

Table 2
Variables considered, their base values and ranges, and corresponding angle of repose

Name of variable	Symbol	Base value	Variable range	Angle of repose (°)
Number of particles	N	2000[a]	–	–
Time step	Δt	$10^{-6} - 5 \times 10^{-5}$ s	–	–
Particle diameter	d	10 mm	2–10 mm	[38, 28]
Rolling friction coefficients	$\mu_{r,pp}$	0.05 mm	0–0.1 mm	[0, 34]
	$\mu_{r,pw}$	$2\mu_{r,pp}$	0–0.2 mm	[0, 30]
Sliding friction coefficients	$\mu_{s,pp}$	0.4	0–0.6	[0, 33]
	$\mu_{s,pw}$	$1.5\mu_{s,pp}$	0–0.6	[0, 28]
Container thickness	ξ ($=w/d$)	4d	4d–24d	[28, 19]
Density	ρ	2500 kg/m^3	500–5000 kg/m^3	[27, 31]
Poisson ratio	v	0.3	0.1–0.7	[26, 30]
Young's modulus	E	2.16×10^6 N/m^2	10^5–10^8 N/m^2	27 ± 1
Damping coefficient	c ($c_t = c_n$)	0.4	0.1–0.8	28 ± 1

[a] N increases as ξ increases.

4. Results and discussion

4.1. Numerical results

Essentially, all the variables listed in Table 2 can affect the angle of repose except for the time-step that is mainly used to control the numerical stability. However, trial simulations indicated that the angle of repose slightly increases as particle density or Poisson ratio increases, and has no obvious change with damping coefficient and Young's modulus for the ranges considered (Table 2). The discussion below is therefore only focused on the variables that have significant effects on the angle of repose.

4.1.1. Effect of rolling and sliding frictions

Rolling and sliding frictions provide a most effective mechanism to control the translational and rotational motions and largely determine the individual contact stability in a sandpile. Therefore, they have significant effects on the angle of repose. To quantify the effect of rolling and sliding friction coefficients on the angle of repose, simulations were conducted for 10-mm spherical particles.

Fig. 2 shows the relationship between the angle of repose and particle–particle rolling friction coefficient $\mu_{r,pp}$ for different sliding friction coefficients. Obviously, increasing $\mu_{r,pp}$ can increase the angle of repose for a given sliding friction coefficient and particle size. Similar trends have also been observed for other sized particles. The rolling friction coefficient between particle and wall $\mu_{r,pw}$ is also an important parameter and gives a torque resistant to the rotational motion of particles on the middle plate and front and rear walls of the container. As shown in Fig. 3, increasing $\mu_{r,pw}$ can significantly increase the angle of repose. Figs. 2 and 3 suggest that the rolling friction between particles $\mu_{r,pp}$ and the rolling friction between particle and wall $\mu_{r,pw}$ are both important in controlling

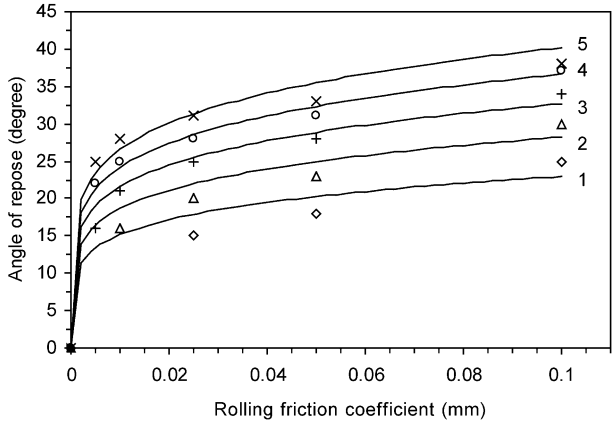

Fig. 2. Angle of repose as a function of rolling friction coefficient with different sliding friction coefficients. Markers are simulation results; solid lines are calculated results by Eq. (3): □ and line 1, $\mu_{s,pp}=0.2$; △ and line 2, $\mu_{s,pp}=0.3$; + and line 3, $\mu_{s,pp}=0.4$; ○ and line 4, $\mu_{s,pp}=0.5$; × and line 5, $\mu_{s,pp}=0.6$.

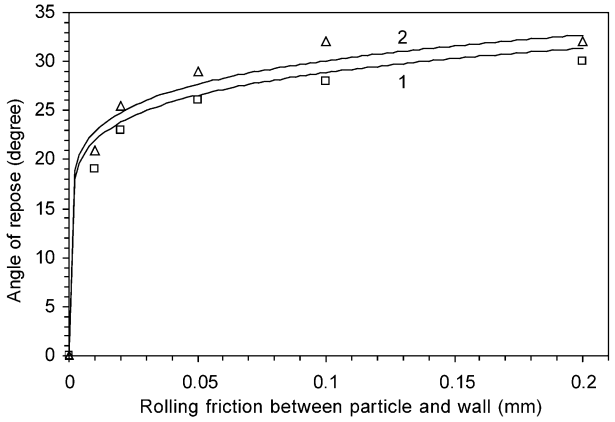

Fig. 3. Angle of repose as a function of rolling friction coefficient between particle and wall with $\mu_{s,pp}=0.4$ and different $\mu_{r,pp}$. Markers are simulation results; solid lines are calculated results by Eq. (3): □ and line 1, $\mu_{r,pp}=0.05$ mm; △ and line 2, $\mu_{r,pp}=0.1$ mm.

the angle of repose. This is because a large rolling friction coefficient means a large resistance force to the rotational motion of spheres, which provides an effective mechanism to consume the kinetic energy and stop the rotational motion of spheres, leading to the formation of a sandpile of high potential [11].

Sliding friction governs the translational motion of particles. A large sliding friction coefficient can tolerate a large magnitude of the elastic deformation in the tangential direction and enhance the stability of individual contacts amongst particles and between particle and wall. Therefore, the effect of sliding friction coefficient is similar to that of rolling friction coefficient. That is, a large sliding friction coefficient between particle and particle $\mu_{s,pp}$ gives a large angle of repose. This is indeed the case as shown in Fig. 4. The angle of repose is also influenced significantly by the sliding friction coefficient between particle and wall $\mu_{s,pw}$ as shown in Fig. 5. No stable heap can be formed without sliding friction between particles and the (bottom) wall. The numerical results are consistent with the previous experimental observation that the angle of repose is obviously higher on a high frictional surface than on a smooth surface [16]. In practice, a high sliding coefficient is often coupled with a high rolling friction coefficient, although the latter should be related to particle shape. The results in Figs. 2–5 suggest that both friction coefficients affect the stability of a sandpile and their proper combination is key to generating results comparable to those physically measured.

4.1.2. Effect of particle size

The effect of particle size on the angle of repose has been studied by a number of investigators with a general conclusion that increasing particle size will decrease the angle of repose [12–14]. This relationship has also been observed in the present study, as shown in Fig. 6. However, it appears that the significance of this size effect varies with simulation

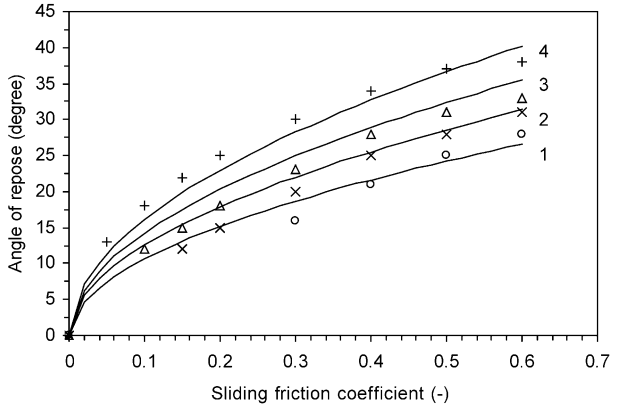

Fig. 4. Angle of repose as a function of sliding friction coefficient with different rolling friction coefficients. Markers are simulation results and solid lines are calculated results by Eq. (3): ○ and line 1, $\mu_{r,pp}=0.01$ mm; × and line 2, $\mu_{r,pp}=0.025$ mm; △ and line 3, $\mu_{r,pp}=0.05$ mm; + and line 4, $\mu_{r,pp}=0.1$ mm.

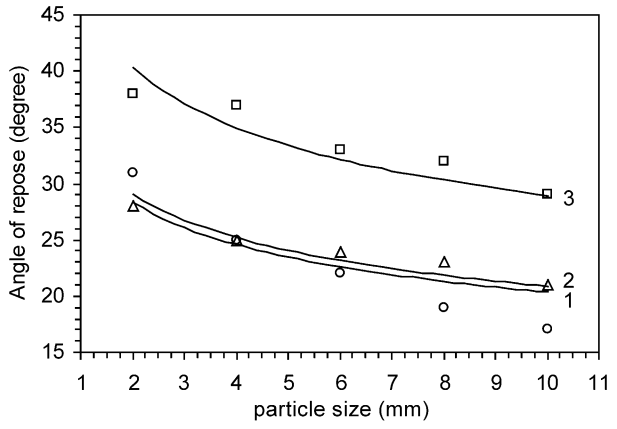

Fig. 6. Angle of repose vs. particle size, with $w/d=4$ and different $\mu_{s,pp}$ and $\mu_{r,pp}$. Markers are simulated results and solid lines are calculated results by Eq. (3): ○ and line 1, $\mu_{r,pp}=0.05$ mm and $\mu_{s,pp}=0.2$; △ and line 2, $\mu_{r,pp}=0.01$ mm and $\mu_{s,pp}=0.4$; □ and line 3, $\mu_{r,pp}=0.05$ mm and $\mu_{s,pp}=0.4$.

conditions, the sliding and rolling friction coefficients in particular.

Carstensen and Chan [13] suggested that the size effect is related to two factors: particle cohesive force and sliding friction coefficient. In particular, under the assumptions that the cohesive force is proportional to particle size and the coefficient of sliding friction decreases with particle size, these authors obtained an equation to relate the angle of repose to particle size. However, their approach does not apply to the present study that concerns with coarse, cohesionless spheres and uses constant sliding and rolling friction coefficients in quantifying the effect of particle size. In fact, the analysis of the numerical results indicates that for coarse spheres, particle size affects the angle of repose mainly through its effect on rolling friction rather than sliding friction [25].

4.1.3. Effect of container thickness

The front and rear walls of the container set up an additional constraint to limit the mobility of particles in contact with the walls, which can propagate into the particle assembly to affect the angle of repose. Figs. 3 and 5 show that changing rolling or sliding friction coefficient between particle and wall changes varies the angle of repose, implying that the front and rear walls, like the bottom wall, also have their effect here.

To quantify this effect, simulations were performed using different container thickness. Fig. 7 shows that increasing the container thickness w decreases the angle of repose for given simulation conditions. However, when the thickness is larger than a critical value, about 20 particle diameter, a constant angle of repose can be obtained, this corresponding

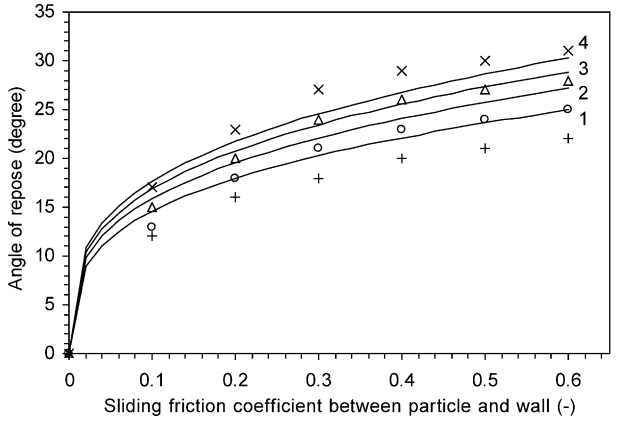

Fig. 5. Angle of repose as a function of sliding friction coefficient between particle and wall with $\mu_{r,pp}=0.05$ mm and different $\mu_{s,pp}$. Markers are simulation results and solid lines are calculated results by Eq. (3): + and line 1, $\mu_{s,pp}=0.2$; ○ and line 2, $\mu_{s,pp}=0.3$; △ and line 3, $\mu_{s,pp}=0.4$; marker × and line 4, $\mu_{s,pp}=0.5$.

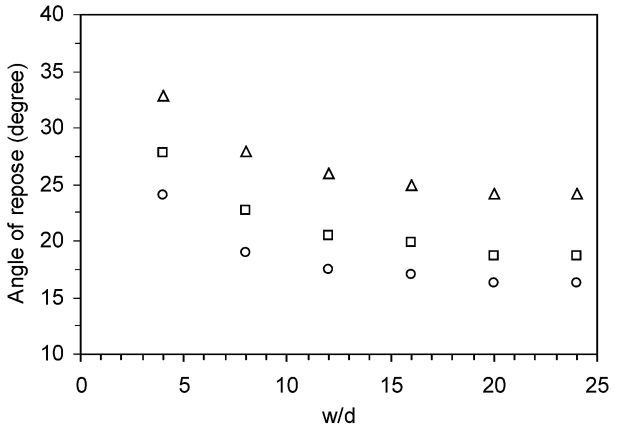

Fig. 7. Angle of repose against container thickness (w/d): △, □ and ○ are numerical results with $\mu_{r,pp}=0.025$ mm and $\mu_{s,pp}=0.4$: △, $d=2$ mm; □, $d=5$ mm; ○, $d=10$ mm.

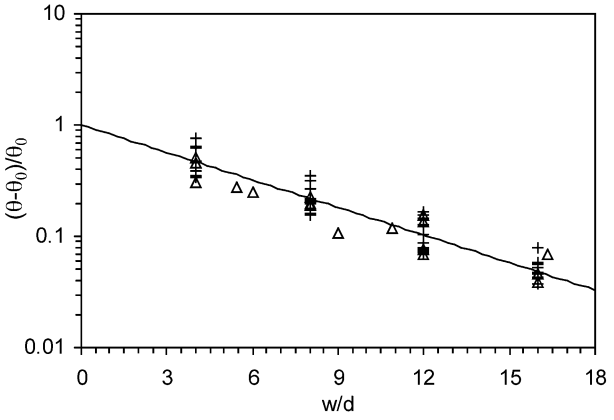

Fig. 8. $(\theta-\theta_0)/\theta_0$ vs. w/d: △, experimental results ($d=0.55$, 1, 2, 5 and 10 mm); +, simulated results for different sized particles ($d=2$, 5 and 10 mm) and different sliding and rolling friction coefficients ($\mu_{s,pp}=0.1-0.6$ and $\mu_{r,pp}=0.01-0.1$ mm).

to a situation without any front and rear wall effect. The simulated results with periodic boundaries applied to the front and rear walls are very close to the angles of repose at the container thickness of 20d. The trend is very much similar to that observed by Grasselli and Herrmann [15] who recently studied this effect for spheres ranging from 112 to 400 μm in size. These authors, however, observed a much larger critical container thickness (equal to about 180 particle diameter). This difference can be attributed to different experimental conditions in size range and inter-particle forces. The cohesive force between particles, which can result from the van der Waals force for dry particles less than 100 μm or the capillary force for humidified particles, affect the piling behaviour of particles significantly [13,16,26–28].

4.2. Formulation of a predictive equation

The proceeding discussion clearly demonstrates that the angle of repose θ is affected by variables such as sliding friction coefficients $\mu_{s,pp}$ and $\mu_{s,pw}$, rolling friction coefficients $\mu_{r,pp}$ and $\mu_{r,pw}$, particle size d, and container thickness w. For sandpiles formed with a thickness 4d, the numerical results can be well described by the following equation:

$$\theta^* = 102 \times \mu_{s,pp}^{0.27} \times \mu_{s,pw}^{0.22} \times \mu_{r,pp}^{0.06} \times \mu_{r,pw}^{0.12} \times d^{-0.2}. \quad (3)$$

The good agreement between the calculated and simulated results shown in Figs. 2–6 confirms the applicability of this equation in the range studied. Actually, the resulting standard deviation is about 2 degrees, almost within the measurement error of the angle of repose.

However, Eq. (3) is only applicable when the thickness of a container is 4d. Changing the thickness will change the angle of repose considerably. It has been reported that the relationship between the angle of repose and the container thickness can be described by an exponential law [15]:

$$\theta = \theta_0(1 + \alpha e^{-kw}) \quad (4)$$

where α and k are parameters that depend on particle characteristics and material properties, θ_0 is the angle of repose without front and rear wall effect, theoretically obtained when $w=+\infty$. As shown in Fig. 8, fitting this equation to the present numerical results gives that $\alpha=1$ and $k=0.18/d$. In this case, substituting Eq. (3) into Eq. (4) and re-arranging the resulting equation give:

$$\theta_0 = 68.61 \times \mu_{s,pp}^{0.27} \times \mu_{s,pw}^{0.22} \times \mu_{r,pp}^{0.06} \times \mu_{r,pw}^{0.12} \times d^{-0.2}. \quad (5)$$

This equation can predict the angle of repose in three dimensions without the effect of container thickness. Eq. (4), facilitated by Eq. (5), can be used to calculate the angle of repose with a finite thickness. As shown in Fig. 9, the calculated angle of repose well matches the simulated one for the conditions given in Table 2. While the absolute error is constant, about 3°, a large relative error may result from these equations when the angle of repose is small.

4.3. Experimental validation

To examine the validity of the proposed simulation technique, physical experiments were carried out under conditions similar to those used in the simulation. The effects of particle friction coefficients are difficult to be measured by physical experiments. Therefore, in this work, we focused on two variables: container thickness and particle size. Figs. 10 and 11 show the typical sandpiles constructed by physical experiments and numerical simulations with different container thicknesses. Note that the

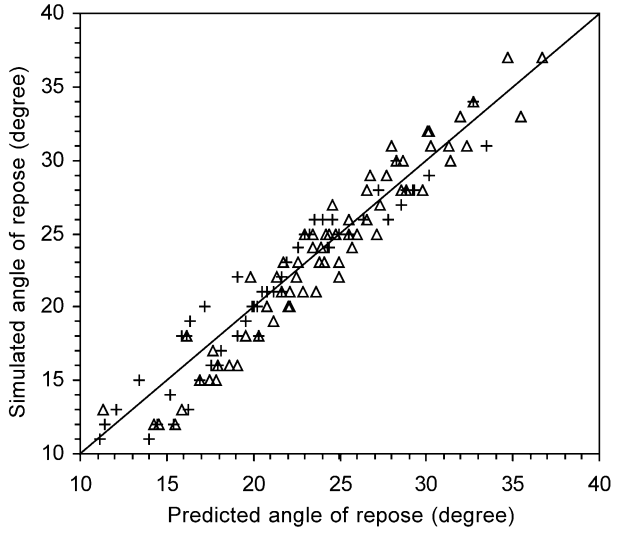

Fig. 9. Predicted vs. simulated angle of repose: △, $w=4d$; +, $w=8d$, 12d, 16d and 20d.

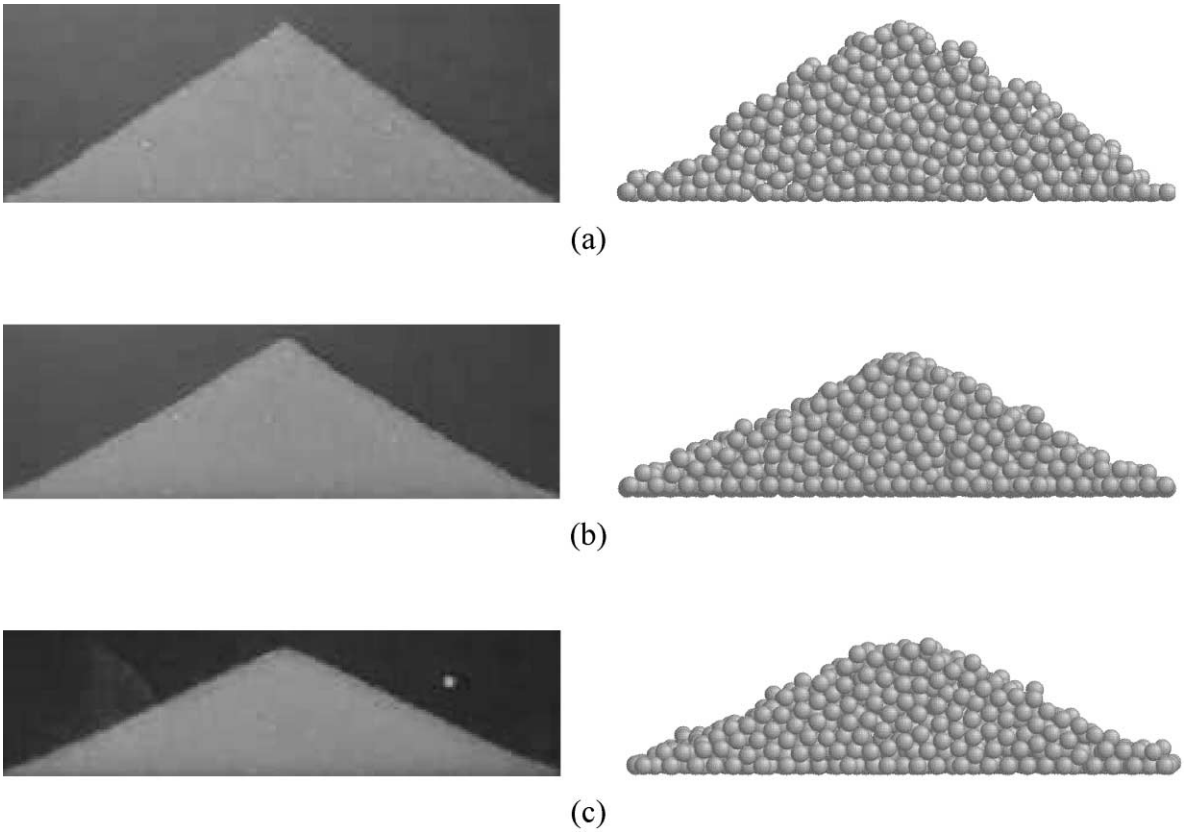

Fig. 10. Sandpiles generated via physical (left column) and numerical (right column, $\mu_{r,pp} = 0.05$ mm and $\mu_{s,pp} = 0.4$) experiments by using 2-mm glass beads with different container thicknesses: (a), $w = 4d$; (b), $w = 12d$; (c), $w = 20d$.

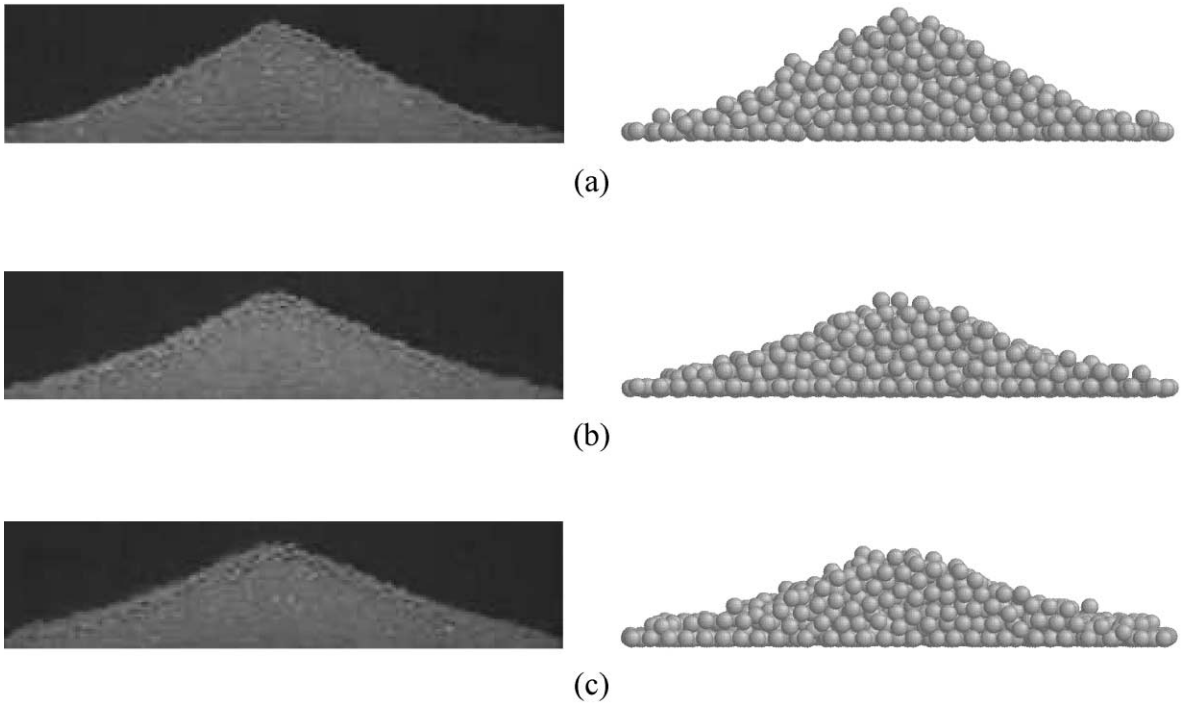

Fig. 11. Sandpiles generated via physical (left column) and numerical (right column, $\mu_{r,pp} = 0.05$ mm and $\mu_{s,pp} = 0.4$) experiments by using 5-mm glass beads with different container thicknesses: (a), $w = 4d$; (b), $w = 12d$; (c), $w = 20d$.

numerical and experimental results were obtained from different-sized containers although they appear to be of the same size in the two figures. Because of the relatively small number of particles, the numerical simulation sometimes does not produce a sandpile of smooth surface. Nevertheless, the results in Figs. 10 and 11 clearly indicate that the angle of repose decreases with increasing container thickness or particle size, and the numerical simulations and physical experiments are quite comparable.

According to Eq. (4), the plot of $(\theta-\theta_0)/\theta_0$ against container thickness w should give a straight line. Fig. 12 shows that indeed this is the case for both physical and numerical results for different sized particles. In particular, the numerical results have a good agreement with the experimental results when $\mu_{r,pp}=0.05$ mm and $\mu_{s,pp}=0.4$. As implied by Fig. 8, the change of μ_r or μ_s does not change the trend much. Parameter k in Eq. (4) is the slope of a line in Fig. 12. Obviously, k depends on particle size. Both physical and numerical experiments suggest that k increases with the decrease of particle size for the range considered, as shown in Fig. 13. This is contrary to the observation of Grasselli and Herrmann [15] that parameter k is independent of particle size. This result can be due to the different experimental conditions as they used much smaller particles with humidity (20–30%). Further study is probably necessary to clarify this issue.

Fig. 14 shows the measured angle of repose θ_0, together with those in the literature [13], as a function of particle size d. It can be shown that the relationship between θ_0 and d can be well described by the power law: $\theta_0=29.6d^{-0.206}$ for particle size ranging from 0.05 to 10 mm. Obviously, the power in this equation is very close to that in Eq. (3) or Eq. (5) obtained based on the numerical results.

The use of the above equations implies a need to quantify properly the sliding and rolling friction coefficients, in addition to particle size. These parameters may be coupled and some are difficult to measure. For example, the dependence of rolling friction coefficient on particle size is still an open and active research area [29–31]. One suggestion is that the rolling friction coefficient may be proportional to particle diameter [29]. If this is the case, the power of d will be reduced from -0.2 to -0.02 according to Eq. (3) or Eq. (5), suggesting that particle size does not so significantly affect the angle of repose for coarse, cohesionless spheres. Nonetheless, it is believed that these equations, while pointing to the future research needs, can at least provide a useful guide for the control of the angle of repose and the internal friction of granular materials. As demonstrated below, while direct evaluation is most desirable, these parameters can be readily estimated through simple physical experiment.

According to Eq. (5), in addition to particle size, other variables will also affect the angle of repose. Comparison of the physical and numerical results suggests that $\mu_{r,pp}=0.05$

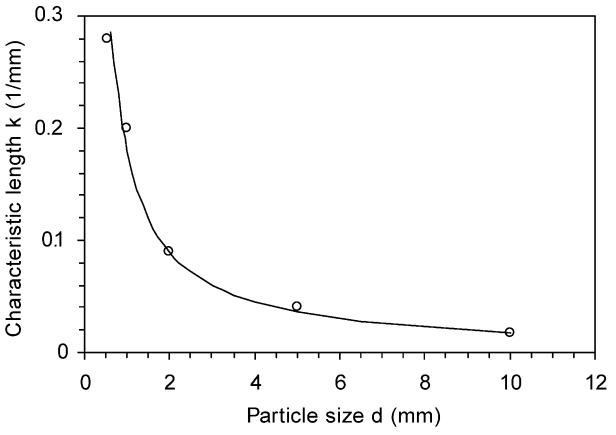

Fig. 13. Characteristic length, k, versus particle size, d; ○, experimental results; solid line, calculated results ($k=0.18/d$).

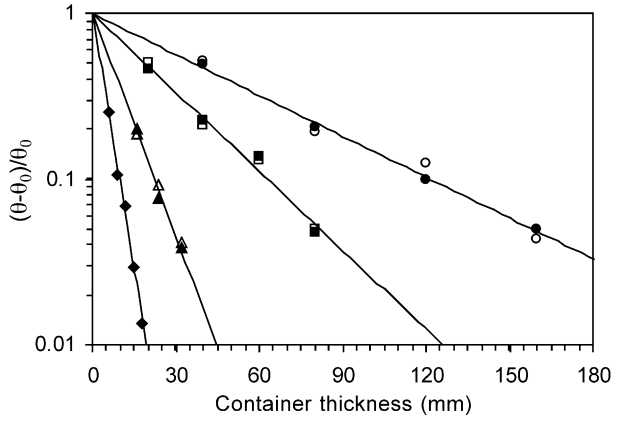

Fig. 12. $(\theta-\theta_0)/\theta_0$ vs. container thickness w for particles of different sizes. Filled markers are experimental results using spherical glass beads; unfilled markers are numerical results with $\mu_{s,pp}=0.4$ and $\mu_{r,pp}=0.05$ mm: ♦, $d=1$ mm; ▲△, $d=2$ mm; ■□, $d=5$ mm; ●○, $d=10$ mm. Solid lines are fitted exponential lines by using the experimental results with particle size $d=1$, 2, 5, 10 mm.

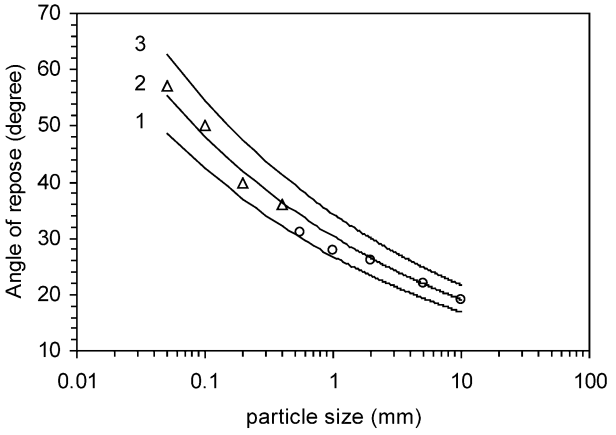

Fig. 14. Angle of repose against particle size: △, experimental results of Carstensen and Chan [13]; ○, present experimental results; solid lines, calculated results by Eq. (5): line 1, $\mu_{s,pp}=0.3$, $\mu_{r,pp}=0.05$ mm; line 2, $\mu_{s,pp}=0.4$, $\mu_{r,pp}=0.05$ mm; line 3, $\mu_{s,pp}=0.4$, $\mu_{r,pp}=0.1$ mm.

mm and $\mu_{s,pp} = 0.4$ is reasonable for glass beads used in this study. Interestingly, this set of parameters has also been found to give results comparable to those measured by means of positron emission particle tracking in a cylindrical bladed mixer [32]. Therefore, it appears that for a given material, glass beads here, there should be one set of parameters that can be generally used in DEM simulations, as theoretically expected. As shown in Fig. 14 also, the calculated angle of repose by Eq. (5) with the use of this set of parameters matches the measured one well. This further confirms the validity of the proposed simulation technique and equations.

5. Conclusions

(1) Sliding and rolling frictions between particles and between particle and wall are the primary factors of controlling the translational and rotational motion of a particle and hence the formation of a sandpile; the angle of repose increases with the increase of either rolling or sliding friction coefficient. The angle of repose decreases with the increase of particle size.

(2) The relationship between the angle of repose and the container thickness can be described by the exponential law proposed by Grasselli and Herrmann [15]. The characteristic length, k, in this law is not a constant but decreases with particle size for cohesionless particles.

(3) The angle of repose for sandpiles formed by discharging method can be estimated by Eqs. (3)–(5) as a function of key variables such as sliding and rolling friction coefficients, the container thickness and particle size for the varying ranges considered.

(4) Comparison between the simulated and experimental results under comparable conditions further confirms the proposed DEM-based simulation technique is a valid method to study the formation of sandpiles and the angle of repose.

List of symbols

c	damping coefficient
d	particle diameter, m
E	Young's modulus, Pa
$\boldsymbol{F}_c$	contact force, N
$\boldsymbol{F}_d$	damping force, N
$\boldsymbol{g}$	acceleration due to gravity (vector, magnitude = 9.81), m/s^2
$\boldsymbol{G}$	gravity (vector), N
I	moment of inertia of particle, kg·m^2
m	mass of particle, kg
$\boldsymbol{M}$	rolling friction torque, N·m
N	number of particles
$\boldsymbol{R}$	radius vector (from particle center to a contact point), m
R	magnitude of $\boldsymbol{R}$, m
$S^2_{\boldsymbol{R}}$	$p \cdot q/N$
Δt	time step, s
t	time, s
$\boldsymbol{T}$	driving friction torque, N·m
$\boldsymbol{V}$	velocity vector, m/s

Greek letters

ρ	particle density, kg/m^3
$\boldsymbol{\delta}$	vector of the accumulated tangential displacement, m
δ	magnitude of $\boldsymbol{\delta}$, m
μ_r	coefficient of rolling friction, m
μ_s	coefficient of sliding friction
ν	Poisson's ratio
$\boldsymbol{\omega}$	angular velocity vector, rad/s
ω	magnitude of angular velocity, m/s
$\hat{\boldsymbol{\omega}}$	unit angular velocity

Subscripts

ij	between particles i and j
i, j	corresponding to ith, jth particle
max	maximum
n	in normal direction
t	in tangential direction

Acknowledgements

The authors are grateful to Australian Research Council and BHP for the financial support of this project.

References

[1] J. Lee, Avalanches in (1 + 1)-dimensional piles—a molecular dynamics study, Journal de Physique I 3 (1993) 2017.
[2] V. Frette, K. Christensen, A. Malthesorenssen, J. Feder, T. Jossang, P. Meakin, Avalanche dynamics in a pile of rice, Nature 379 (1996) 49.
[3] H. Jaeger, C. Liu, S. Negel, Relaxation at the angle of repose, Physical Review Letters 62 (1989) 40.
[4] H.A. Makse, Stratification instability in granular flows, Physical Review A: Atomic, Molecular, and Optical Physics 56 (1997) 7008.
[5] J. Baxter, U. Tuzun, D. Heyes, I. Hayati, P. Fredlund, Stratification in poured granular heaps, Nature 391 (1998) 136.
[6] R. Jullien, P. Meakin, A. Pavlovitch, Particle size segregation by shaking in 2-dimensional disc packings, Europhysics Letters 22 (1993) 523.
[7] V. Buchholtz, T. Poschel, Numerical investigations of the evolution of sandpiles, Physica A 202 (1994) 390.
[8] C.M. Dury, G.H. Ristow, J.L. Moss, M. Nakagawa, Boundary effects on the angle of repose in rotating cylinders, Physical Review A: Atomic, Molecular, and Optical Physics 57 (1998) 4491.
[9] J. Lee, H.J. Herrmann, Angle of repose and angle of marginal stability: molecular dynamics of granular particles, Journal of Physics A 26 (1993) 373.
[10] K.M. Hill, J. Kakalios, Reversible axial segregation of rotating granular media, Physical Review A: Atomic, Molecular, and Optical Physics 52 (1995) 4393.
[11] Y.C. Zhou, B.D. Wright, R.Y. Yang, B.H. Xu, A.B. Yu, Rolling friction in the dynamic simulation of sandpile formation, Physica A 269 (1999) 536.

[12] A. Burkalow, Angle of repose and angle of sliding friction: an experimental study, Bulletin of The Geological Society of America 56 (1945) 669.
[13] J. Carstensen, P. Chan, Relation between particle size and repose angles of powder, Powder Technology 15 (1976) 129.
[14] M. Carrigy, Experiments on the angles of repose of granular materials, Sedimentology 14 (1970) 147.
[15] Y. Grasselli, H.J. Herrmann, On the angles of dry granular heaps, Physica A 246 (1997) 301.
[16] H. Kalman, D. Goder, M. Rivken, G. Ben-Dor, The effect of the particle–surface friction coefficient on the angle of repose, Bulk Solids Handling 13 (1993) 123.
[17] R. Jullien, P. Meakin, A mechanism for particle size segregation in three dimensions, Nature (London) 344 (1990) 425.
[18] P. Meakin, R. Jullien, Simple models for two and three dimensional particle size segregation, Physica A 180 (1992) 1.
[19] A. Mehta, G.C. Barker, Disorder, memory and avalanches in sandpiles, Europhysics Letters 27 (1994) 501.
[20] A. Mehta, G.C. Barker, The dynamics of sand, Reports on Progress in Physics 57 (1994) 383.
[21] P.A. Cundall, O.D.L. Strack, A discrete numerical model for granular assemblies, Geotechnique 29 (1979) 47.
[22] K. Yamane, M. Nakagawa, S.A. Altobelli, T. Tanaka, Y. Tsuji, Steady particulate flows in a horizontal rotating cylinder, Physics of Fluids 10 (1998) 1419.
[23] T. Elperin, E. Golshtein, Comparison of different models for tangential forces using the particle dynamics method, Physica A 242 (1997) 332.
[24] D. Tabor, Mechanics of rolling friction II, Proceedings of the Royal Society of London, Series A: Mathematical, Physical and Engineering Sciences 229 (1955) 198.
[25] Y.C. Zhou, B.H. Xu, A.B. Yu, P. Zulli, A numerical investigation of the angle of repose of mono-sized spheres, Physical Review E: Statistical Physics, Plasmas, Fluids, and Related Interdisciplinary Topics 64 (2001) 021301.
[26] N. Standish, A. Yu, Q. He, An experimental study of packing of a coal heap, Powder Technology 68 (1991) 187.
[27] L. Bocquet, E. Charlaix, S. Ciliberto, J. Crassous, Moisture-induced ageing in granular media and the kinetics of capillary condensation, Nature 396 (1998) 735.
[28] N. Fraysse, H. Thome, L. Petit, Humidity effects on the stability of a sandpile, European Physical Journal B: Condensed Matter Physics 11 (1999) 615.
[29] H. Soodak, M.S. Tiersten, Perturbation analysis of rolling friction on a turntable, American Journal of Physics 64 (1996) 1130.
[30] N.V. Brilliantov, T. Poschel, Rolling friction of a viscous sphere on a hard plane, Europhysics Letters 42 (1998) 511.
[31] N.V. Brilliantov, T. Poschel, Rolling as a ''continuing collision'', European Physical Journal B: Condensed Matter Physics 12 (1999) 299.
[32] R.L. Stewart, J. Bridgwater, Y.C. Zhou, A.B. Yu, Simulated and measured flow of granules in a bladed mixer—a detailed comparison, Chemical Engineering Science 56 (2001) 5449.